

S. Bouraghda, K. Sebaa, M. Bechouat, M. Sedraoui

## An improved sliding mode control for reduction of harmonic currents in grid system connected with a wind turbine equipped by a doubly-fed induction generator

**Introduction.** The implementation of renewable energy resources into the electrical grid has increased significantly in recent years. Wind power is one of the existing resources. Presently, power electronics has become an indispensable tool in wind power plants. **Problem.** However the associated control usually has an impact on increasing the harmonic distortion, especially on the output voltage. **Goal.** This paper proposes a new sliding mode control strategy, applied on a rotor-side of a doubly-fed induction generator. The main goal is to meet the electrical power requirements, while responding to the power quality issues. **Methodology.** The wind energy conversion system must be able to not only track the maximum power point of the wind energy, but also to mitigate the harmonic currents caused by the non-linear loads. To achieve this goal, the power converters are driven by the proposed sliding mode control strategy. The corresponding two gains of the sliding surface are well selected using a particle swarm optimization algorithm. The particle swarm optimization algorithm solves a constrained optimization problem whose fitness function is a prior formulated as the sum of two mean square error criterions. The first criterion presents the tracking dynamic of the reference active power while the second one presents the tracking dynamic of the reference reactive power. **The novelty** lies in the implementation of the particle swarm optimization algorithm in conventional sliding mode control strategy, in which the proposed-improved sliding mode control strategy is developed. The wind energy conversion system control uses the principal of the vector oriented control to decouple the control of the active power from that of the reactive power. **Results.** The improved sliding mode control strategy is applied to control separately these powers in the presence of non-linear loads. The energy assessment of this strategy is analysed using the wind energy conversion system model based on SimPower software. **Originality.** The obtained simulation results confirm the superiority of the proposed-improved sliding mode control strategy in terms of reference tracking dynamics and suppression of harmonic currents. References 23, tables 2, figures 11.

**Key words:** doubly-fed induction generator; wind energy conversion system; bidirectional converter; particle swarm optimization; sliding mode control.

**Вступ.** Використання відновлюваних джерел енергії в електричній мережі останніми роками значно зросло. Енергія вітру – один із існуючих ресурсів. Нині силова електроніка стала незамінним інструментом вітряних електростанцій. **Проблема.** Проте, відповідне управління зазвичай має вплив на збільшення гармонійних спотворень, особливо у вихідній напрузі. **Мета.** У цій статті пропонується нова стратегія управління ковзним режимом, що застосовується на боці ротора асинхронного генератора з подвійним живленням. Основна мета – задовольнити вимоги до електроенергії, вирішуючи відповідні проблеми з якістю електроенергії. **Методологія.** Система перетворення енергії вітру повинна мати можливість не тільки відстежувати точку максимальної потужності вітру, але й пом'якшувати гармонійні струми, викликані нелінійними навантаженнями. Для досягнення цієї мети силові перетворювачі керуються запропонованою стратегією управління ковзним режимом. Відповідні два коефіцієнти посилення поверхні ковзання добре вибираються з використанням алгоритму оптимізації рою частинок. Алгоритм оптимізації рою частинок вирішує задачу оптимізації з обмеженнями, функція придатності якої заздалегідь сформульована як сума двох критеріїв середньоквадратичної похибки. Перший критерій репрезентує динаміку відстеження еталонної активної потужності, а другий – динаміку відстеження еталонної реактивної потужності. **Новизна** полягає в реалізації алгоритму оптимізації рою частинок у традиційній стратегії управління ковзним режимом, в якій розроблена запропонована покращена стратегія управління ковзним режимом. Управління системою перетворення енергії вітру використовує принцип векторно-орієнтованого управління, щоб відокремити управління активною потужністю від управління реактивною потужністю. **Результати.** Удосконалена стратегія управління ковзним режимом застосовується для роздільного управління цими потужностями за наявності нелінійних навантажень. Енергетична оцінка цієї стратегії аналізується за допомогою моделі системи перетворення енергії вітру на основі програмного забезпечення SimPower. **Оригінальність.** Отримані результати моделювання підтверджують перевагу запропонованої удосконаленої стратегії управління ковзним режимом з точки зору еталонної динаміки стеження та придушення гармонійних струмів. Бібл. 23, табл. 2, рис. 11.

**Ключові слова:** асинхронний генератор із подвійним живленням; система перетворення енергії вітру; двонаправлений перетворювач; оптимізація рою частинок; керування ковзним режимом.

### Abbreviations

APF	Active Power Filter	PRC	Proportional Resonance Control
BTB	Back-To-Back	PSO	Particle Swarm Optimization
DFIG	Doubly-Fed Induction Generator	PWM	Pulse-Width Modulation
DPC	Direct Power Control	RSC	Rotor-Side Converter
DTC	Direct Torque Control	SMC	Sliding Mode Control
GSC	Grid-Side Converter	THD	Total Harmonic Distortion
HSF	High Selectivity Filter	VCS	Vector Control Scheme
MPP	Maximum Power Point	VOC	Vector Oriented Control
MSE	Mean Square Error	WECS	Wind Energy Conversion System
NLL	Non-Linear Loads	WPP	Wind Power Plants
PMSG	Permanent Magnet Synchronous Generator	WT	Wind Turbine

**Introduction.** The incorporation of renewable energy resources into the electrical grid has increased significantly in recent years. Among of them, the wind

energy is one of the existing resources whose potential demand has increased due to domestic and industrial

© S. Bouraghda, K. Sebaa, M. Bechouat, M. Sedraoui

necessities. This growth is mainly due to the advanced technology used in the design of WECS, reducing the cost of producing electrical energy and enabling it to be competitive with other traditional sources such as fossil fuels, petroleum, natural gas, and so on. A lot of research has focused on DFIG systems in their structures. These have several advantages, including speed control, current harmonic reduction and four-quadrant active and reactive power control. As its rotor speed can be operated at any wind speed, the DFIG system is therefore able to deliver high mechanical power and, in economic terms, it becomes more attractive than other existing conversion systems, thanks to its conversion rate, which is generally around 30% of the nominal power, allowing thus to generate the electrical energy at a lower cost [1].

Currently, power electronics has become an indispensable tool in WPPs to ensure such required specifications such as steady state stability, high energy efficiency, regardless of changing wind conditions. In fact, these tools are often providing many important functionalities to WTs, including the control of several electrical quantities such as stator terminal voltage and frequency, active and reactive power and so on. Nevertheless, the associated control effort usually has an impact on increasing the harmonic distortion, especially on the output voltage of existing converters. As a result, the occurrence of inadequate harmonics has unfortunately become the main issue for the majority of wind energy designers as well as the company managers [2]. The attenuation of the effect of such harmonics on the DFIG system can be performed through proper regulation of the existing converters in the control loop. Similarly, the power quality problem can also be posed of serious challenges where its remedy has been discussed by several researchers [1, 2]. On these grounds, many control strategies have been proposed to overcome these drawbacks. Among them, a control strategy was published in [3] where the WECS is designed to operate partially as an active filter. Also, another control strategy that can be employed to simultaneously generate active and reactive power where an extra active filter is incorporated into a DFIG wind system having a variable speed [1]. Similarly, a modulation technique was proposed in [4] for shunt active filter operation, in which the existing harmonics in the WECS output current are well mitigated. The corresponding feedback control system incorporates a PMSG as well as an AC/DC current converter. Also, a PWM control strategy including a five-leg converter was proposed in [5] where the given performances are compared by those provided by the conventional six-leg topology. The main shortcoming, compared to the six-leg BTB converter, lies in the restriction of increasing the DC link voltage for the same operating point. In parallel, a PRC strategy was developed in [6] for a stationary reference frame to mitigate, as much as possible, the existing harmonics in the rotor current and in torque pulsations. In the same direction, a VCS was suggested in [7, 8] for rotor-side control of a stand-alone generator based on a wound rotor induction machine. The main aim of the proposed control scheme is to keep a constant terminal voltage with stationary frequency at the generator output. In the same way, the

full harmonic component compensation technique of the grid current was adopted in [9]. The corresponding RSC control structure is modified, in which a filtering task is incorporated. Also, an efficiency assessment of the electrical part of the WECS was reported in [10] where the two BTB-PWM inverters, which are supplied with voltage and connected between the stator and rotor, are used to improve the bidirectional power flow. Accordingly, the second inverter, which is disposed on the grid side, serves as an active power filtering to remove the harmonics, generated by the nonlinear load, while providing the required active and reactive power to the DFIG rotor.

Different alternative control strategies have been developed for wind power generation in the electrical grid. Among them, the VOC and the two direct control strategies such as the DTC and the DPC are becoming the most widely used in real world applications [11]. Furthermore, some other nonlinear control strategies have been proposed in the literature where the best known is the SMC, which has proven to be the most attractive during the last decades. This is due to its inherent properties to overcome complex challenges that are caused by the presence of unmolded dynamics, the neglect of high frequency dynamics, the presence of model uncertainties, the variation of model parameters, the presence of load disturbances, and the persistence of the effect of sensor noise. To this purpose, it is important to emphasize that the SMC-based synthesis of a robust controller, taking into account all the previous obstacles, is crucial for the active and reactive power control of the DFIG equipped with a wind turbine [12]. Nevertheless, this control strategy has the capacity to provide good reference tracking dynamics, high robustness in the presence of the preceding factors, and a good tradeoff between the two preceding targets. However, it also presents various misfunctions when strict specifications are considered. Among them, the undesired phenomenon known as «chattering» occurs during the operation of the WECS near its operating point. The drawback that results from this phenomenon is often associated with improper selection of sliding surface gains where trial and error selection is typically performed, leading thus to control inaccuracy, dramatic performance degradation and high thermal loss in power devices. To overcome this problem, the PSO algorithm is introduced in the conventional-SMC-based synthesis where their gains are properly optimized. This can be done by solving the constrained optimization problem whose fitness function is perfectly minimized. The manner of the incorporation of the PSO algorithm in conventional SMC strategy constitutes therefore the main contribution of this paper.

**Goal.** In this paper, the actual behavior of WECS is primarily modelled near its operating point. Then, the VOC principal is used for decoupling the active power control from the reactive power one. Finally, the improved-SMC-based synthesis is applied to ensure the proper reference tracking dynamics where the suppression of harmonic currents is considered.

**System description.** The WECS is mainly composed by a DFIG equipped with a wind turbine. Its stator is connected to the grid while the BTB PMW

converter is connected between the DFIG rotor and the grid. The grid-side converter GSC is used to provide bi-directional power flow that is generated from the rotor-side converter RSC, stabilizing thus the DC link voltage and achieving unity power factor. Figure 1 shows the block diagram of a grid-connected DFIG wind turbine.

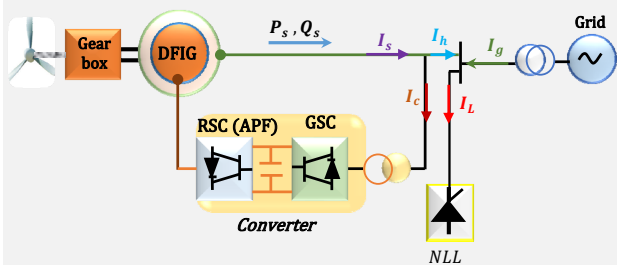


Fig. 1. Block diagram of the grid connected DFIG wind turbine in the presence of NLL

In general, the NLL often unfortunately injects harmonic current into the grid where the desired controller for active and reactive power regulations must be operated as an active filter, in which the existing harmonic currents and voltages are well absorbed. Also, from Fig. 1, the node law imposes that:

$$I_g = I_L - I_h; \quad (1)$$

$$I_h = I_s - I_c. \quad (2)$$

The stator current  $I_s$  of the DFIG is assumed to have a non-sinusoidal waveform close to that of the NLL current  $I_L$ . The converter is designed to supply a pure sinusoidal current  $I_c$ . Then, the harmonic current  $I_h$  thus represents the current that the APF (rotor converter) must generate. Therefore, and in accordance with (1), the grid current  $I_g$  will be clear of unwanted harmonic components. To be in agreement with these assumptions, the suggested WECS must generate the same harmonic components as the non-linear current but with opposite phases. This may be performed by investigating the correct control circuit of the rotor converter. Keep in mind that this control circuit may also be used to achieve decoupled control of active and reactive power. The NLL currents must be measured. Following that, the measured load currents ( $I_{La}$ ,  $I_{Lb}$ ,  $I_{Lc}$ ) are converted using the  $abc$  to  $\alpha\beta$  (stationary reference frame) transformation. The NLL current is equal to the sum of the fundamental frequency and various harmonics, as shown below:

$$I_{L\alpha} = I_{L\alpha f} + I_{L\alpha h}; \quad (3)$$

$$I_{L\beta} = I_{L\beta f} + I_{L\beta h}, \quad (4)$$

where ( $I_{L\alpha h}$ ,  $I_{L\beta h}$ ) and ( $I_{L\alpha f}$ ,  $I_{L\beta f}$ ) are the NLL current's harmonic and fundamental constituents.

Based on (3), (4) and by deducting the load current from its fundamental component, the harmonic components of the NLL current can be expressed. The approach depicted in Fig. 2 can be utilized to distinguish the harmonic of NLL. In this figure, the Park transformation is applied to convert the  $\alpha\beta$  current components to  $d-q$  (synchronous) reference frame. The HSF is used to extract the fundamental component from  $\alpha\beta$  components. The HSF is a band pass filter as in Fig. 2 [8].

It should be noted that the design of the controller design based on the SMC strategy for tracking both

reference active and reference reactive powers requires prior modeling of all parts involved in the actual WECS behavior, such as wind-turbine part, the rotor-side and stator-side of the converter.

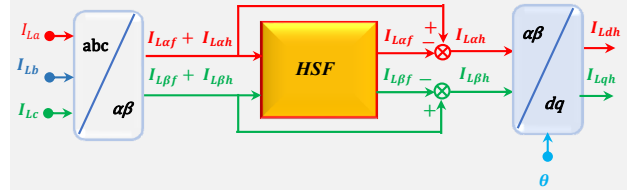


Fig. 2. Harmonic isolation of the whole load harmonic current

**Modeling of actual WECS behavior. Modeling of wind turbine.** A wind turbine collects the wind through its blades and transmits it to the rotor hub. The kinetic energy of the wind is accordingly converted into mechanical power, generating thus a mechanical torque. Also, the rotor shaft generates an electrical energy and transmits it to the grid. Since the wind energy is found in the form of kinetic energy where its amplitude depends on the air density and the wind speed [12, 13]. The power of the wind  $P_v$  being found in the form of kinetic energy when it crosses at the speed  $V_v$ , air density  $\rho$  and the surface area  $S$ . It can be expressed by:

$$P_v = \frac{1}{2} \cdot \rho \cdot S \cdot V_v^3. \quad (5)$$

The wind turbine can usually only recuperate a part of the preceding power  $P_v$ , resulting thus the power  $P_t$  that is expressed by:

$$P_t = \frac{1}{2} \cdot \rho \cdot \pi \cdot R^2 \cdot V_v^3 \cdot C_p, \quad (6)$$

where  $R$  is the radius of the wind turbine;  $C_p$  is the corresponding power coefficient, which is given as a function of the wind speed, the rotation speed and the pitch angle.

Also,  $C_p$  is often given as a function of the tip speed ratio  $\lambda$ , which is defined by:

$$\lambda = \frac{\Omega_t \cdot R}{V_v}, \quad (7)$$

where  $\Omega_t$  is the angular speed of the rotor.

Furthermore, the wind power  $P_t$  and the power extracted by the wind turbine  $P_v$  are expressed in terms of the power coefficient  $C_p$ . Hence, one can obtain:

$$P_t = \frac{1}{2} \cdot C_p(\lambda, \beta) \cdot \rho \cdot S \cdot V_v^3, \quad (8)$$

where the coefficient  $C_p(\lambda, \beta)$  has a theoretical limit, called BETZ limit. It is defined by:

$$C_p(\lambda, \beta) = C_1 \cdot \left( \frac{C_2}{\lambda_i} - C_3 \cdot \beta - C_4 \right) e^{\frac{-C_5}{\lambda_i}} + C_6 \cdot \lambda. \quad (9)$$

The numerical values of the parameters  $C_k$  are experimentally given by:

$$C_1 = 0.5176; C_2 = 116; C_3 = 0.4; C_4 = 5; C_5 = 21; C_6 = 0.0068, \quad (10)$$

while the parameter  $\lambda_i$  is expressed by:

$$\frac{1}{\lambda_i} = \frac{1}{(\lambda + 0.08 \cdot \beta)} - \frac{0.035}{\beta^3 + 1}. \quad (11)$$

It is worth noting here that the power conversion coefficient  $C_p$  is expressed as a function of the tip speed



occurred between the reference current  $i_{dg}^*$  and the current  $i_{dg}$ . It allows to regulate the active power  $P_g$  of the grid. Similar, the  $i_{qg}$  regulator is used to control the reactive power  $Q_g$  of the grid, in which the difference  $i_{qg}^* - i_{qg}$  is removed [16].

For better performance in the dynamic responses, there is additionally one coupling component in each equation that is best incorporated in the control as a feed-forward term, as illustrated in Fig. 5 (at the output of the current controllers) [16]:

$$e_{df} = -\omega_s \cdot L_f \cdot i_{qg}; \quad (21)$$

$$e_{df} = \omega_s \cdot L_f \cdot i_{dg}. \quad (22)$$

**Design controller for RSC** The rotor-side converter is designed to control the DFIG output power to grid. It is also used to control the power factor across the DFIG [1]. The stator active and reactive powers serve as the control inputs of the RSC. As mentioned previously, the aim is to operate the DFIG as an APF. The SMC strategy is used for the RSC where the block diagram of RSC is shown in Fig. 6.

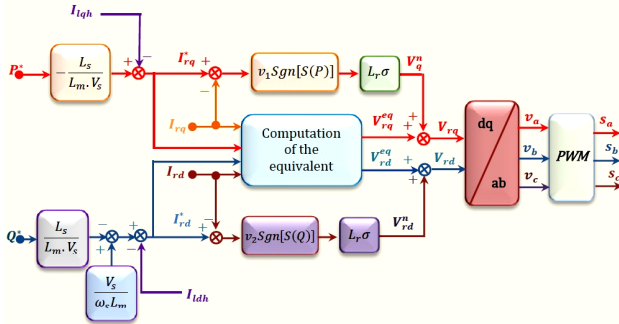


Fig. 6. Control loop performed in the rotor-side converter

Assuming that a reference frame is rotating synchronously with the stator flux and we suppose that the network is stable, the stator flux  $\psi_{sd}$  is becoming constant and equal to  $\psi_s$ . On the other hand, the stator flux  $\psi_{sq}$  becomes zero, i.e.,  $\psi_{sd} = \psi_s$ ,  $\psi_{sq} = 0$ . Also, for the generators utilized in the wind turbine the stator resistance  $R_s$  may be ignored, resulting in  $V_{sd} = 0$  and  $V_{sq} = V_s = \omega_s \cdot \psi_{sq}$ .

**Conventional SMC strategy** The SMC strategy is a very powerful nonlinear tool that has been widely employed by researchers, especially in the last decades [15, 17]. It consists in moving the system behavior along a predetermined sliding surface, where a numeric control signal is applied [12]. Moreover, the state trajectory of the closed-loop system must be oriented towards the sliding surface  $S(x) = 0$  and maintained constantly around this surface using the switching logic function  $U^n$ . In general, the basic SMC law is commonly expressed by [18, 19]:

$$U_c = U^{eq} + U^n, \quad (23)$$

where  $U^{eq}$  is the equivalent control law that is applied when the existing states of the system are located in the slip plane.

The control law  $U^n$  is alternated between  $-k$  and  $+k$  where  $k > 0$ . It is defined by:

$$U^n = k \cdot \text{sgn}[S(x)]. \quad (24)$$

Also, the sigmoid function occurred in (24) is defined by:

$$\text{sgn}[S(x)] = \begin{cases} -1 & \text{if } S(x) < 0; \\ 1 & \text{if } S(x) > 0. \end{cases} \quad (25)$$

According to the SMC principal, the control law  $U^n$  has often stabilized the WECS behavior, in which the given power conversion becomes maximal and the corresponding speed ratio reaches its optimal point  $\lambda_{opt}$ . This closed-loop stability requires often to satisfy the Lyapunov condition that is expressed by:

$$S(x) \cdot \dot{S}(x) < 0, \quad (26)$$

where  $\dot{S}(x) = \frac{dS(x)}{dt}$  denotes the derivative of the sliding surface, which is expressed as a function of the variable to be controlled ( $x$ ). This last will be considered as either the active power or the reactive power that is delivered by the WECS.

The goal is first to decouple the control of the active power  $P_s$  from that of the reactive power  $Q_s$ . Then, the desired controller based on the conventional SMC strategy should keep good track of both reference powers  $P_s^*$  and  $Q_s^*$ , in which a proper suppression of all harmonics occurring in the duty currents should be taken into account. These requirements need detailing some equations such as the rotor currents and their derivatives as well as the sliding surfaces and their derivatives. Furthermore, the relationships between reference stator powers and the reference rotor currents are given by:

$$I_{rq}^* = \frac{-L_s}{V_s \cdot L_m} \cdot P_s^* - I_{Lqh}; \quad (27)$$

$$I_{rd}^* = \frac{V_s}{\omega_s \cdot L_m} - \frac{L_s}{V_s \cdot L_m} \cdot Q_s^* - I_{Ldh}. \quad (28)$$

Noted here, that the reference reactive power  $Q_s^*$  is set to zero and the reference active power  $P_s^*$  can be expressed is related to the synchronous speed  $\omega_s$ , and the electromagnetic torque  $T_{em}$  can be expressed by:

$$P_s^* = \Omega_s \cdot T_{em}. \quad (29)$$

Moreover, the derivative of rotor currents, in  $d$ -axis and  $q$ -axis, are expressed by:

$$\frac{dI_{rq}}{dt} = \frac{1}{L_r \cdot \sigma} \left( V_{rq} - R_r \cdot I_{rq} - g \cdot \omega_s \cdot L_r \cdot \sigma \cdot I_{rd} - g \cdot \omega_s \cdot \frac{L_m \cdot V_s}{\omega_s \cdot L_s} \right); \quad (30)$$

$$\frac{dI_{rd}}{dt} = \frac{1}{L_r \cdot \sigma} \left( V_{rd} - R_r \cdot I_{rd} + g \cdot \omega_s \cdot L_r \cdot \sigma \cdot I_{rq} \right),$$

where  $g$  and  $\sigma$  are respectively the slip and dispersion coefficient.

In general, the active power becomes directly proportional to the rotor current in  $q$ -axis, while the reactive power becomes proportional to the rotor current in  $d$ -axis. Accordingly, the control surface of each power is expressed by:

$$S(P) = I_{rq}^* - I_{rq}; \quad (31)$$

$$S(Q) = I_{rd}^* - I_{rd}. \quad (32)$$

Knowing that the appropriate reference tracking dynamics necessitates that all sliding surfaces as well as their derivatives must be equal to zero, i.e.,  $S(P) = 0$ ,  $S(Q) = 0$ ,  $\dot{S}(P) = 0$  and  $\dot{S}(Q) = 0$ . These require that the

plot of  $P_s$  (with respect to  $Q_s$ ) is exponentially converged to the one of the corresponding reference powers  $P_s^*$  (with respect to  $Q_s^*$ ). Therefore, all previous sliding surfaces necessarily become attractive and invariant, where the key to the success of the SMC strategy strongly depends on respecting the attractivity relationship of Lyapunov [17], given by (26).

**Control law used for active power control** This part focuses on finding the two parts of the control law  $V_{rq}^{eq}$  (equivalent control vector) and  $V_{rq}^n$  (switching part of the control) that constituting the rotor voltage  $V_{rq}$ , given in  $q$ -axis. Accordingly, the derivative of the sliding surface  $\dot{S}(P)$  is computed using (30)-(32), which yields also (33) as follow:

$$\dot{S}(P) = \frac{-L_s}{L_m \cdot V_s} \cdot \dot{P}_s^* - \dot{I}_{Ldh} - \frac{1}{L_r \cdot \sigma} \left( V_{rq} - R_r \cdot I_{rq} - g \cdot \omega_s \cdot L_r \cdot \sigma \cdot I_{rd} - g \cdot \frac{L_m \cdot V_s}{L_s} \right) \quad (33)$$

From (33) the control law  $V_{rq}$  is determined and then decomposed into the two control laws  $V_{rq}^{eq}$  and  $V_{rq}^n$ , where  $V_{rq} = V_{rq}^{eq} + V_{rq}^n$ . The resulting rotor voltages in  $q$ -axis are given by:

$$V_{rq} = \frac{-L_s \cdot L_r \cdot \sigma}{L_m \cdot V_s} \cdot \dot{P}_s^* - \dot{I}_{Ldh} + R_r \cdot I_{rq} + g \cdot \omega_s \cdot L_r \cdot \sigma \cdot I_{rd} + g \cdot \frac{L_m \cdot V_s}{L_s} + L_r \cdot \sigma \cdot v_1 \cdot \text{sgn}[S(P)] \quad (34)$$

$$V_{rq}^{eq} = \frac{-L_s \cdot L_r \cdot \sigma}{L_m \cdot V_s} \cdot \dot{P}_s^* - \dot{I}_{Ldh} + R_r \cdot I_{rq} + g \cdot \omega_s \cdot L_r \cdot \sigma \cdot I_{rd} + g \cdot \frac{L_m \cdot V_s}{L_s}; \quad (35)$$

$$V_{rq}^n = L_r \cdot \sigma \cdot v_1 \cdot \text{sgn}[S(P)]. \quad (36)$$

#### Control law used for reactive power control

Similarly, the derivative of the sliding surface  $\dot{S}(Q)$  is first computed and the control law  $V_{rd}$  is then extracted as follows:

$$\dot{S}(Q) = \left( \frac{V_s}{L_m \cdot \omega_s} - \frac{L_s}{L_m \cdot V_s} \cdot \dot{Q}_s^* - \dot{I}_{Ldh} \right) - \frac{1}{L_r \cdot \sigma} \left( V_{rd} - R_r \cdot I_{rd} + g \cdot \omega_s \cdot L_r \cdot \sigma \cdot I_{rq} \right) \quad (37)$$

$$V_{rd} = L_r \cdot \sigma \left( \frac{V_s}{L_m \cdot \omega_s} - \frac{L_s}{L_m \cdot V_s} \cdot \dot{Q}_s^* - \dot{I}_{Ldh} \right) + R_r \cdot I_{rd} - g \cdot \omega_s \cdot L_r \cdot \sigma \cdot I_{rq} + L_r \cdot \sigma \cdot v_2 \cdot \text{sgn}[S(Q)] \quad (38)$$

According to (38), the two control laws  $V_{rd}^{eq}$  and  $V_{rd}^n$  are expressed by:

$$V_{rd}^{eq} = L_r \cdot \sigma \left( \frac{V_s}{L_m \cdot \omega_s} - \frac{L_s}{L_m \cdot V_s} \cdot \dot{Q}_s^* - \dot{I}_{Ldh} \right) + R_r \cdot I_{rd} - g \cdot \omega_s \cdot L_r \cdot \sigma \cdot I_{rq}; \quad (39)$$

$$V_{rd}^n = L_r \cdot \sigma \cdot v_2 \cdot \text{sgn}[S(Q)]. \quad (40)$$

The block diagram that explains the SMC implementation for active and reactive power controls of the DIFG equipped with a wind turbine is given in Fig. 6.

From (38), (40), it is obvious that the desired reference tracking dynamic requires the proper interaction of all states of the system toward the switching surfaces, i.e.,  $S(P) = 0$  and  $S(Q) = 0$ . This still leads to the occurrence of the chattering problem due to the existing of the sigmoid function in both control laws  $V_{rq}^n$  and  $V_{rd}^n$ , in which the control law  $V_{rq}^n$  can either have the

gain  $-v_1$  or  $+v_1$ . In the other hand, the control law  $V_{rd}^n$  can either have the gain  $-v_2$  or  $+v_2$ . To overcome this challenge, the implementation of the PSO algorithm to optimize the two gains appearing in the two preceding control laws becoming an indispensable key in the design phase of the controllers. This enables to highlight the improved version of the SMC strategy whose details are discussed in the next part.

**Improved SMC strategy** In this study, the main contribution lies in the selection of the two optimal gains  $v_1$  and  $v_2$  involved in the two control laws  $V_{rq}^n$  and  $V_{rd}^n$  respectively. The corresponding bounded optimization problem includes the fitness function  $J(X)$ , expressed as the MSE criterion. It consists of the sum of the two squared errors  $e_1$  and  $e_2$ , produced by the simultaneous tracking of the two reference powers  $P_s^*$  and  $Q_s^*$ . Accordingly, the optimization problem can be expressed by:

$$\min_{X_{\min} \leq X \leq X_{\max}} J(X) = \min_{X_{\min} \leq X \leq X_{\max}} \left\{ \frac{1}{NT} \sum_{i=1}^N [e_1^2(X) + e_2^2(X)] \right\} \quad (41)$$

where both tracking errors  $e_1$  and  $e_2$  are defined by  $e_1(X) = P_s(X) - P_s^*$  and  $e_2(X) = Q_s(X) - Q_s^*$  respectively,  $X = (X_1, X_2)^T$  denotes the design vector to be optimized where their components are constrained by  $-v_1 \leq X_1 \leq +v_1$  and  $-v_2 \leq X_2 \leq +v_2$ ,  $N$  and  $T$  denote the total number of samples and the sampling time.

The PSO algorithm is implemented in a classical SMC strategy to avoid the fast switching of the two gains  $v_1$  and  $v_2$  from their positive to their negative values. In fact, there is a multitude of unknown gains found between the two positive and negative bounds for each gain of the sliding surface. The objective is therefore mainly to focus on finding the optimal gains during the tracking process of the two reference powers. These optimal gains lead to finding two feasible optimal commands, in which the chattering problem of the SMC strategy is well solved. The optimization process by the PSO algorithm is carried out as follows: The PSO algorithm uses a swarm made up of particles  $n_p \in N$  to know in search of the sub-optimal solution  $X^* \in N^{q \times 1}$  which minimizes the objective function, called  $J(X) \in R$ . The position and velocity of particle vectors  $i^{\text{th}}$  are given respectively by  $X_i = (X_{i,1}, X_{i,2}, \dots, X_{i,q})^T$  and  $V_i = (V_{i,1}, V_{i,2}, \dots, V_{i,q})^T$ . They are determined by the following iterative expressions [20-22]:

$$\begin{aligned}
V_i^{l+1} &= c_0 \cdot V_i^l + c_1 \cdot r_{1,i}^l \cdot (X_i^{best,l} - X_i^l) + \\
&+ c_2 \cdot r_{2,i}^l \cdot (X_{swarm}^{best,l} - X_i^l); \\
X_i^{l+1} &= X_i^l + V_i^{l+1},
\end{aligned} \quad (42)$$

where  $l$  is the number of iterations previously provided by the user;  $c_0$ ,  $c_1$  and  $c_2$  are respectively the inertia factor, the cognitive (individual) and social (group) learning relationships;  $r_{1,i}^l$  and  $r_{2,i}^l$  are random numbers evenly distributed over the interval  $[0, 1]$ ,  $X_i^{best,l}$  and  $X_{swarm}^{best,l}$  are respectively the best position obtained previously by the particle and the best position obtained in the whole of the swarm at the current iteration  $l$ . In summary, the PSO algorithm can consist of the following steps [21-23]:

- **Step 1:** initialize the  $n_p$  particles with positions chosen at random and which should previously be contained in the lower and upper bound vector  $X_{min}$  and  $X_{max}$ ;
- **Step 2:** evaluate the fitness function for each position;
- **Step 3:** determine the initial solutions  $X_i^{best,0}$  and  $X_{swarm}^{best,0}$ ;
- **Step 4:** check the stop condition. If it is satisfied, the algorithm then converges to the desired optimal gains  $v_1^{opt}$  and  $v_2^{opt}$ . Otherwise, go to the next step;
- **Step 5:** assign the new values obtained to all particles (updates);
- **Step 6:** go back to step 2.

It should be noted that the PSO algorithm is achieved by obtaining the two optimal gains  $v_1^{opt}$  and  $v_2^{opt}$ . They are multiplied by the constant value  $L_r \cdot \sigma$  and then used for computing the two optimal commands  $V_{rq}^{n,opt}$  and  $V_{rd}^{n,opt}$ . Knowing that the two equivalent commands such as  $V_{rq}^{eq}$  and  $V_{rd}^{eq}$  are a priori computed using (35), (39), respectively. The resulting four preceding optimal commands are used to compute the two optimal rotor voltages  $V_{rq}^{opt}$  and  $V_{rd}^{opt}$  using (34), (38), respectively.

**Simulation results and discussion.** The previous system (Fig. 1) was modelled and simulated using SimPower System Demo, MATLAB/Simulink. The proposed control strategy is applied to a WECS equipped with a 2MW DFIG. The system parameters are presented in the Appendix 1. The optimal values obtained are  $V_1 = 1550.05211$  and  $V_2 = 525.0299$  as shown in the fitness plots (Fig. 7) provided by the algorithm during the extraction process for 20 execution of the code.

Figure 8 is the simulation results for active and reactive power response in case of sliding mode control. In this case study, simulation results show clearly the improvement of active and reactive power demand obtained by applying sliding mode control in term of time response and good reference tracking accuracy.

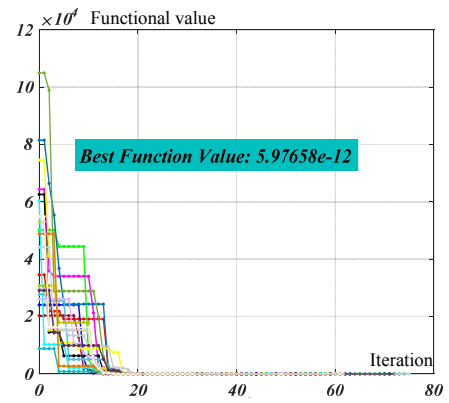


Fig. 7. The obtained fitness curve through PSO

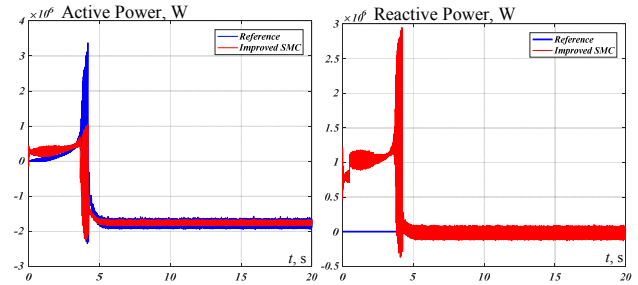


Fig. 8. Active and reactive powers

The most significant harmonic components which will spread in the grid side with a THD as depicted in Fig. 9. After implementing the active filtering technique on the rotor current control loop, the waveform became greatly improved with better harmonic spectrum as displayed in Fig. 10. Referring to the results obtained, THD values are put in the table below (Table 1). The grid side inverter gives an active and reactive power needed by the rotor of DFIG.

Table 1

THD of the grid current	
THD without filtering, %	THD after filtering, %
26.22	2.45

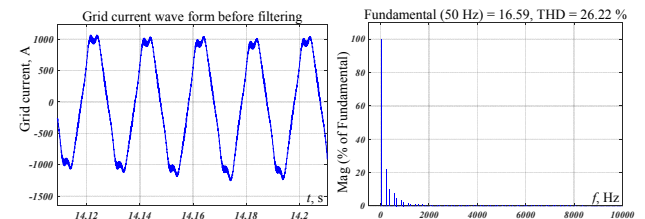


Fig. 9. Grid current wave form and his harmonic spectrum before filtering

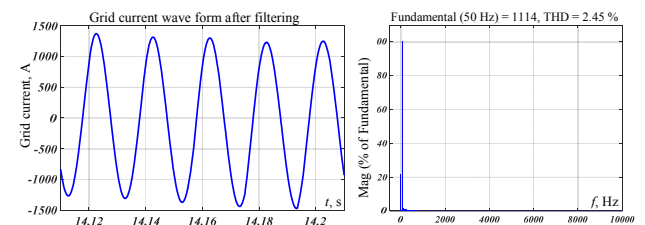


Fig. 10. Grid current wave form and his harmonic spectrum after filtering

The reference harmonic compensating currents is shown in Fig. 10. Concerning  $V_{dc}$  regulation, the obtained result is satisfying. In fact, as illustrated in Fig. 11, after a transient state,  $V_{dc}$  follows perfectly its reference ( $V_{ref} = 1190$  V).

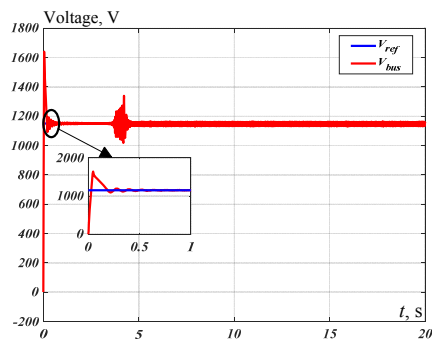


Fig. 11. DC-bus voltage wave form

## Conclusions.

In this article, a study concerning a wind turbine based on a doubly-fed induction generator connected to the grid has been elaborated. The goals were to implement a rotor current control loop that would eliminate harmonic currents generated from a coupled nonlinear load using an active filtering concept, while also permitting independent regulation of power flow from and to the generator. For this reason, rotor converter was used as an active power filter. The response was conclusive given the improvements (an almost sinusoidal shape) obtained in the network current. Where we

have found that the total harmonic distortion decrease from 26.22 % (before filtering) to 2.45 % (after filtering).

In addition, the other goal was to regulate the common DC bus voltage between the rotor converter and the grid converter. In this study, we discovered that the simulation results show clearly the improvement of active and reactive power demand obtained by applying sliding mode control in term of time response and good reference tracking accuracy.

In summary, the following characteristics of the proposed wind energy conversion system are highlighted in the following points:

1. Possibility to recover the maximum quantity of power from the input wind speed.
2. Using an active power filter to reduce the harmonic currents.

Finally, in order to complete the suggested investigation, the power factor must be corrected. Additionally, the system should be implemented on a real machine in order to explore the impact of the saturation effect on the performance of the generator. These considerations will be investigated in future work.

**Conflict of interest.** The authors declare that they have no conflicts of interest.

## Appendix 1

System parameters [16]

Turbine			DFIG		
Parameter	Value	Parameter	Value		
Radius, m	42	Speed range, rpm	900-2000		
Nominal wind speed, m/s	12.5	Pole pairs	2		
Optimum tip speed ratio $\lambda_{opt}$	7.2	Magnetizing inductance $L_m$ , mH	2.5		
Maximum power coefficient $C_{pmax}$	0.44	Rotor leakage inductance $L_r$ , $\mu$ H	87		
Air density $\rho$ , kg/m <sup>3</sup>	1.1225	Stator leakage inductance $L_s$ , $\mu$ H	87		
Inertia $J$ , kg-m <sup>2</sup>	127	Rotor resistance $R_r$ , m $\Omega$	26		
Friction $D$ , N-m-s/rad	0.001	Stator resistance $R_s$ , m $\Omega$	29		
DFIG			Grid		
Nominal stator active power, MW	2	Grid inductance $L_g$ , mH	0.4		
Nominal torque, N-m	12732	Grid resistance $R_g$ , m $\Omega$	0.02		
Stator voltage, V	690	Grid frequency $f$ , Hz	50		
Nominal speed, rpm	1500	Grid voltage $V_g$ , V	690		

## REFERENCES

1. Nosratabadi S.M., Gholipour E. Power system harmonic reduction and voltage control using DFIG converters as an active filter. *Turkish Journal of Electrical Engineering & Computer Sciences*, 2016, vol. 24, pp. 3105-3122. doi: <https://doi.org/10.3906/elk-1406-35>.
2. Dhua D., Yang G., Zhang Z., Kocewiak L.H., Timofejevs A. Harmonic Active Filtering and Impedance-based Stability Analysis in Offshore Wind Power Plants. *Proceedings of 16th Wind Integration Workshop*, 2017, pp. 1-8.
3. Mishra A., Tripathi P.M., Chatterjee K. A review of harmonic elimination techniques in grid connected doubly fed induction generator based wind energy system. *Renewable and Sustainable Energy Reviews*, 2018, vol. 89, pp. 1-15. doi: <https://doi.org/10.1016/j.rser.2018.02.039>.
4. Hoseinpour A., Masoud Barakati S., Ghazi R. Harmonic reduction in wind turbine generators using a Shunt Active Filter based on the proposed modulation technique. *International Journal of Electrical Power & Energy Systems*, 2012, vol. 43, no. 1, pp. 1401-1412. doi: <https://doi.org/10.1016/j.ijepes.2012.06.052>.
5. Gonçalves P.F.C., Cruz S.M.A., Mendes A.M.S. Fault-Tolerant Predictive Control of a Doubly-Fed Induction Generator with Minimal Hardware Requirements. *IECON 2018 - 44th Annual Conference of the IEEE Industrial Electronics Society*, 2018, pp. 3357-3362, doi: <https://doi.org/10.1109/IECON.2018.8592825>.
6. Hosseini Mousavi S.N., Barati H. Direct power control simultaneously in the rotor side converter and grid side converter of DFIG for wind turbines with elimination of network current harmonics. *Journal of Novel Researches on Electrical Power*, 2019, vol. 8, no. 3, pp: 37-51. Available at: <http://jeeps.iaud.ac.ir/article-1-229-en.pdf> (Accessed 20 May 2021).
7. Xu W., Yu K., Liu Y., Gao J., Hua W. Improved Harmonics Elimination for Standalone Brushless Doubly-Fed Induction Generator with Nonlinear Loads. *2018 XIII International Conference on Electrical Machines (ICEM)*, 2018, pp. 243-249. doi: <https://doi.org/10.1109/ICELMACH.2018.8506764>.
8. Gaillard A., Poure P., Saadate S., Machmoum M. Variable speed DFIG wind energy system for power generation and harmonic current mitigation. *Renewable Energy*, 2009, vol. 34, no. 6, pp. 1545-1553. doi: <https://doi.org/10.1016/j.renene.2008.11.002>.
9. Kesraoui M., Chaib A., Meziane A., Boulezaz A. Using a DFIG based wind turbine for grid current harmonics filtering. *Energy Conversion and Management*, 2014, vol. 78, pp. 968-975. doi: <https://doi.org/10.1016/j.enconman.2013.07.090>.
10. Mahieddine H., Zarour L., Lamri L., Lokmane N.A. Developing a grid-connected DFIG strategy for the integration of wind power with harmonic current mitigation. *International Journal of Electrical and Computer Engineering (IJECE)*, 2019, vol. 9, no. 5, pp. 3905. doi: <https://doi.org/10.11591/ijece.v9i5.pp3905-3915>.
11. Kadri A., Marzougui H., Bacha F. Implementation of direct power control based on stator flux estimation using low-pass

filter estimator for doubly fed induction generator–wind energy conversion system. *Proceedings of the Institution of Mechanical Engineers, Part I: Journal of Systems and Control Engineering*, 2019, vol. 233, no. 7, pp. 764-778. doi: <https://doi.org/10.1177/0959651818818895>.

12. Rouabhi R., Abdessemed R., Chouder A., Djeriou A. Power Quality Enhancement of Grid Connected Doubly-Fed Induction Generator Using Sliding Mode Control. *International Review of Electrical Engineering (IREE)*, 2015, vol. 10, no. 2, pp. 266. doi: <https://doi.org/10.15866/iree.v10i2.5347>.

13. Kahla S., Bechouat M., Amieur T., Sedraoui M., Babes B., Hamouda N. Maximum power extraction framework using robust fractional-order feedback linearization control and GM-CPSO for PMSG-based WECS. *Wind Engineering*, 2021, vol. 45, no. 4, pp. 1040-1054. doi: <https://doi.org/10.1177/0309524X20948263>.

14. Hamouda N., Benalla H., Hemsas K., Babes B., Petzoldt J., Ellinger T., Hamouda C. Type-2 fuzzy logic predictive control of a grid connected wind power systems with integrated active power filter capabilities. *Journal of Power Electronics*, 2017, vol. 17, no. 6, pp. 1587-1599. doi: <https://doi.org/10.6113/JPE.2017.17.6.1587>.

15. Beltran B., Benbouzid M., Ahmed-Ali T., Mangel H. DFIG-based wind turbine robust control using high-order sliding modes and a high gain observer. *International Review on Modelling and Simulations*, 2011, vol. 4, no. 3, pp. 1148-1155. Available at: <https://hal.archives-ouvertes.fr/hal-00630436v2/document> (Accessed 20 May 2021).

16. Abad G., López J., Rodríguez M.A., Marroyo L., Iwanski G. *Doubly Fed Induction Machine: Modeling and Control for Wind Energy Generation*. John Wiley & Sons, 2011. 625 p. doi: <https://doi.org/10.1002/9781118104965>.

17. Abdellah A., Abdelhafid A., Mostafa R. Combining sliding mode and linear quadratic regulator to control the inverted pendulum. *International Review of Automatic Control*, 2013, vol. 6, no. 1, pp. 69-76. Available at: [https://www.praiseworthyprize.org/jsm/index.php?journal=irea\\_co&page=article&op=view&path%5B%5D=11286](https://www.praiseworthyprize.org/jsm/index.php?journal=irea_co&page=article&op=view&path%5B%5D=11286) (Accessed 20 May 2021).

18. Sadeghi R., Madani S.M., Ataei M., Agha Kashkooli M.R., Ademi S. Super-Twisting Sliding Mode Direct Power Control of a Brushless Doubly Fed Induction Generator. *IEEE Transactions on Industrial Electronics*, 2018, vol. 65, no. 11, pp. 9147-9156. doi: <https://doi.org/10.1109/TIE.2018.2818672>.

19. Radhwane S., Abdelkader M., Salim D., Aissa K. A fuzzy sliding mode robust control for a field oriented dual star induction machine fed by photovoltaic power supply with MPPT algorithm. *Mediterranean Journal of Measurement and*

*Control*, 2016, vol. 12, no. 4, pp. 654-663. Available at: [https://www.researchgate.net/publication/309674107\\_A\\_fuzzy\\_sliding\\_mode\\_robust\\_control\\_for\\_a\\_field\\_oriented\\_dual\\_star\\_in\\_uction\\_machine\\_fed\\_by\\_photovoltaic\\_power\\_supply\\_with\\_M\\_PPT\\_algorithm](https://www.researchgate.net/publication/309674107_A_fuzzy_sliding_mode_robust_control_for_a_field_oriented_dual_star_in_uction_machine_fed_by_photovoltaic_power_supply_with_M_PPT_algorithm) (Accessed 20 May 2021).

20. Zahedi H., Arab Markadeh G., Taghipour S. Real-time implementation of sliding mode control for cascaded doubly fed induction generator in both islanded and grid connected modes. *Journal of Electrical and Computer Engineering Innovations (JECEI)*, 2020, vol. 8, no. 2, pp. 285-296. doi: <https://doi.org/10.22061/jecei.2020.7361.384>.

21. Bechouat M., Younsi A., Sedraoui M., Soufi Y., Youfsi L., Tabet I., Touafek K. Parameters identification of a photovoltaic module in a thermal system using meta-heuristic optimization methods. *International Journal of Energy and Environmental Engineering*, 2017, vol. 8, no. 4, pp. 331-341. doi: <https://doi.org/10.1007/s40095-017-0252-6>.

22. Bechouat M., Soufi Y., Sedraoui M., Kahla S. Energy storage based on maximum power point tracking in photovoltaic systems: A comparison between GAs and PSO approaches. *International Journal of Hydrogen Energy*, 2015, vol. 40, no. 39, pp. 13737-13748. doi: <https://doi.org/10.1016/j.ijhydene.2015.05.008>.

23. Soufi Y., Bechouat M., Kahla S. Fuzzy-PSO controller design for maximum power point tracking in photovoltaic system. *International Journal of Hydrogen Energy*, 2017, vol. 42, no. 13, pp. 8680-8688. doi: <https://doi.org/10.1016/j.ijhydene.2016.07.212>.

Received 12.01.2022

Accepted 14.02.2022

Published 20.04.2022

Skander Bouraghda<sup>1</sup>, PhD, Assistant Professor,

Karim Sebaa<sup>1</sup>, Professor,

Mohcen Bechaoua<sup>2,3</sup>, PhD, Associate Professor,

Moussa Sedraoui<sup>3</sup>, Professor,

<sup>1</sup>Laboratory of Advanced Electronic Systems (LSEA), University of Medea, Algeria,

e-mail: skander21440@yahoo.fr (Corresponding Author), karim.sebaa@gmail.com

<sup>2</sup>Automatic & Electromechanic Department, University of Ghardaia, Algeria, e-mail: mohcene.oui@gmail.com

<sup>3</sup>The Telecommunications Laboratory, 8 Mai 1945 – Guelma University, Alegria, e-mail: sedraoui.moussa@univ-guelma.dz

#### How to cite this article:

Bouraghda S., Sebaa K., Bechouat M., Sedraoui M. An improved sliding mode control for reduction of harmonic currents in grid system connected with a wind turbine equipped by a doubly-fed induction generator. *Electrical Engineering & Electromechanics*, 2022, no. 2, pp. 47-55. doi: <https://doi.org/10.20998/2074-272X.2022.2.08>